



Universiteit
Leiden
The Netherlands

Experimental quantum position verification: practical challenges and single-photon correlations

Kanneworff, K.N.

Citation

Kanneworff, K. N. (2026, February 18). *Experimental quantum position verification: practical challenges and single-photon correlations*. Retrieved from <https://hdl.handle.net/1887/4291850>

Version: Publisher's Version

License: [Licence agreement concerning inclusion of doctoral thesis in the Institutional Repository of the University of Leiden](#)

Downloaded from: <https://hdl.handle.net/1887/4291850>

Note: To cite this publication please use the final published version (if applicable).

3 Polarization in long fibers and modulators

As discussed in the previous chapter, many quantum position verification (QPV) schemes, and particular those which we discuss in this thesis, rely on manipulation and transmission of polarization-encoded photonic qubits. In order to achieve a lab-based experimental demonstration of such a QPV scheme, one needs to be able to simulate long distances, which is most practical using optical fibers. However, polarization states often change when propagating through fiber-based optical components by stress and strain, which can be used for polarization modulation but also appears due to uncontrolled environmental effects. The environmental effects can be mitigated if the polarization state changes unitarily. In this chapter, we investigate the operation and polarization stability of fiber-based polarization modulators used to prepare polarization qubits, and the transport of such qubits through 200 m-long single-mode fibers that will be used for qubit transport between the QPV nodes. First, a general background about polarization optics is discussed, after which we delve into the question of whether or not the action by the fiber-optic elements can be described as unitary transformations. Next, we examine the stability of a fiber-based polarization modulator, followed by an investigation of the long-term polarization stability of a single-mode fiber. The chapter concludes with a discussion and estimation of polarization mode dispersion in an optical fiber.

3.1 General polarization optics

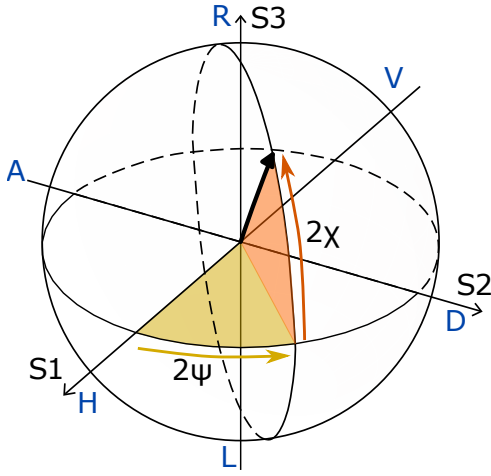


Figure 3.1: Depiction of the Poincaré sphere.

R/L polarization states lie on the x,y, and z axes of the sphere, respectively. Polarization states can also be described by using the Stokes parameters $S_{0...3}$, where S_0 describes the intensity and the Stokes parameters S_1 , S_2 and S_3 give the distribution of the intensity in the $\{H,V\}$, $\{D,A\}$, and $\{R,L\}$ bases, respectively:

$$\begin{aligned} S_0 &= I_H + I_V \\ S_1 &= I_H - I_V \\ S_2 &= I_D - I_A \\ S_3 &= I_R - I_L \end{aligned} \tag{3.1}$$

The Stokes formalism is very useful to describe realistic states of polarization, including not fully polarized (depolarized) light. The Stokes parameters can be related to the spherical coordinate angles (see Fig. 3.1) by using the normalized Stokes parameters s_1 , s_2 and s_3 , where $s_i = S_i/S_0$:

$$\begin{aligned} s_1 &= p \cos(2\chi) \cos(2\psi) \\ s_2 &= p \cos(2\chi) \sin(2\psi) \\ s_3 &= p \sin(2\chi) \end{aligned} \tag{3.2}$$

The angles ψ and χ are the polarization azimuth and ellipticity, respectively, and p denotes the degree of polarization (DOP). We add the zeroth normalized Stokes parameter $s_0 = 1$. We can then express the polarization density matrix with the normalized Stokes parameters using the Pauli matrices σ_1 , σ_2 , and σ_3 , and as the zeroth Pauli matrix the identity matrix $\sigma_0 = I$:

$$\rho = \frac{1}{2} (s_0 \sigma_0 + s_1 \sigma_1 + s_2 \sigma_2 + s_3 \sigma_3) = \frac{1}{2} \begin{pmatrix} s_0 + s_1 & s_2 - i s_3 \\ s_2 + i s_3 & s_0 - s_1 \end{pmatrix} \tag{3.3}$$

Fidelity of polarization states

In this chapter, we want to investigate various polarization effects in a way that is directly relevant for a future QPV experiment. Therefore, we evaluate the polarization behavior

The polarization of light describes the geometrical orientation of the oscillations of, for instance, the electric field vector of light [42]. In a plane transverse to the optical axis, polarization can be described in 3 orthonormal and mutually unbiased bases: the horizontal (H) - vertical (V) basis, the diagonal (D) - anti-diagonal (A) basis, and the right (R) and left (L) circular basis. In the first two linear bases, the field vector oscillates in a plane, while in the circular basis, the field rotates around the optical axis.

The polarization space is visualized by the Poincaré sphere, which is mathematically equivalent to the qubit Bloch sphere, depicted in Fig. 3.1. There, the H/V, D/A,

of optical components not in terms of the Stokes parameters but in terms of fidelities between different polarization states - this provides direct information on the usability of the components for QPV. The fidelity between two quantum states defined by density matrices ρ_1 and ρ_2 is defined by [43]

$$F(\rho_1, \rho_2) = \left(\text{Tr} \sqrt{\sqrt{\rho_1} \rho_2 \sqrt{\rho_1}} \right)^2. \quad (3.4)$$

The square roots are well defined since ρ_1 and ρ_2 are both Hermitian, as seen in Eq. 3.3. Both ρ_1 and ρ_2 have the same definition, for clarity we use $n_0 \dots n_3$ as the normalized Stokes parameters for ρ_2 . By substituting the definition of the density from Eq. 3.3 into Eq. 3.4, we obtain an expression for the fidelity as a function of the Stokes parameters:

$$F(\rho_1, \rho_2) = \frac{1}{4} \left(\sqrt{\Omega - \sqrt{\omega}} + \sqrt{\Omega + \sqrt{\omega}} \right)^2 \quad \text{with} \quad (3.5)$$

$$\Omega = s_0 n_0 + s_1 n_1 + s_2 n_2 + s_3 n_3 \quad \text{and} \quad (3.6)$$

$$\begin{aligned} \omega = & s_0^2 (n_1^2 + n_2^2 + n_3^2) + s_1^2 (n_0^2 - n_2^2 - n_3^2) + s_2^2 (n_0^2 - n_1^2 - n_3^2) + s_3^2 (n_0^2 - n_1^2 - n_2^2) \\ & + 2s_0 s_1 n_0 n_1 + 2s_0 s_2 n_0 n_2 + 2s_0 s_3 n_0 n_3 + 2s_1 s_2 n_1 n_2 + 2s_1 s_3 n_1 n_3 + 2s_2 s_3 n_2 n_3 \end{aligned} \quad (3.7)$$

This result is valid for both pure and mixed polarization states. However, when the states involved are pure ($S_0^2 = S_1^2 + S_2^2 + S_3^2$) i.e. $p = 1$, the expression of ω in Eq. 3.7 reduces to

$$\omega = \sum_{i=0}^3 \sum_{j=0}^3 s_i s_j n_i n_j. \quad (3.8)$$

We now consider several examples illustrating the fidelities between relevant polarization basis states. Specifically, we focus on the three mutually unbiased bases $\{H, V\}$, $\{D, A\}$, and $\{R, L\}$. We choose for ρ_1 the horizontal polarization state H with $s_0 = 1$, $s_1 = 1$, and $s_2 = s_3 = 0$. If ρ_2 is equal to ρ_1 ($\rho_2 = \rho_1$), we naturally find $F(\rho_1, \rho_2) = F(\rho_1, \rho_1) = 1$. If ρ_2 is orthogonal, that is V-polarized, then $n_0 = 1$, $n_1 = -1$ and $n_2 = n_3 = 0$, and we quickly find that the fidelity $F(\rho_1, \rho_2) = 0$, as expected. Finally, if ρ_2 is a basis state in another mutually unbiased basis, for instance diagonally polarized ($n_0 = n_2 = 1$ and $n_1 = n_3 = 0$) it follows that $F(\rho_1, \rho_2) = 1/2$. We summarize:

$$F(\rho_1, \rho_2) = \begin{cases} 1 & \text{for } \rho_1 = \rho_2 \\ 0 & \text{for } \rho_1 \perp \rho_2 \\ 1/2 & \text{for } \rho_1 \text{ and } \rho_2 \text{ basis states of different unbiased bases} \end{cases} \quad (3.9)$$

3.2 Unitary transformation of a long single-mode fiber

In the absence of loss and nonlinear optical effects, within the stationary regime, the polarization transformation by a single-mode fiber is expected to be unitary. This property is crucial for using polarization in quantum communication experiments. Here, we investigate the unitarity of a single-mode fiber experimentally using the setup shown in Fig. 3.2. We use 830 nm laser light (Thorlabs LPS-830-FC) and define its polarization state with a combination of a linear polarizer, a quarter-wave plate, and a half-wave plate before sending it through a 200 m long 780HP single-mode fiber. The polarization state

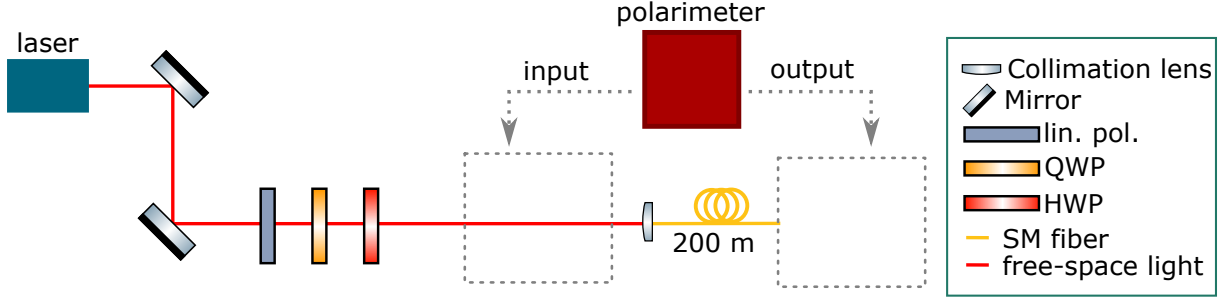


Figure 3.2: Schematic of the experimental setup to measure polarization changes in a 200 m long single-mode optical fiber.

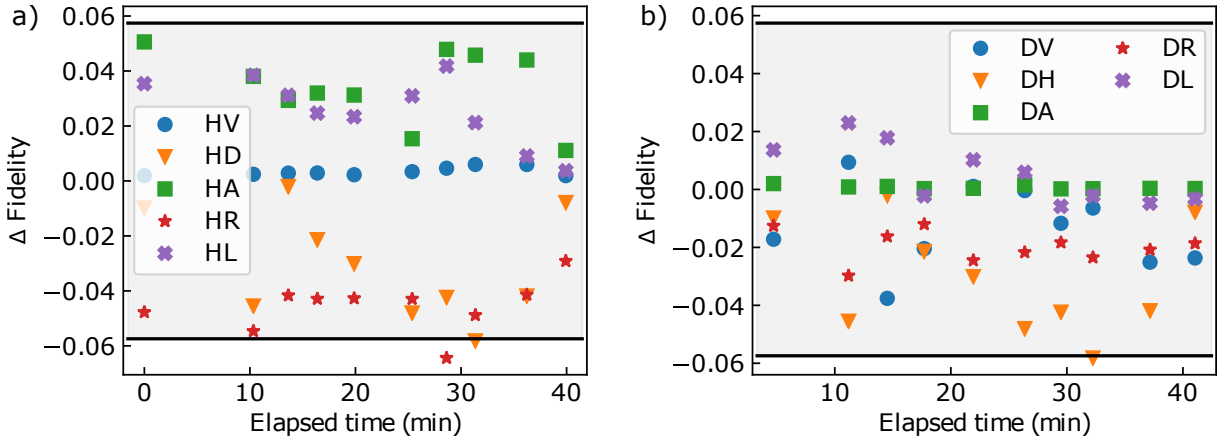


Figure 3.3: The deviation of the measured fidelity after the 200 m fiber from the expected fidelity ΔF as a function of the elapsed time. (a) $\Delta F(\rho_{H,\text{out}}, \rho_{i,\text{out}})$ comparing the H and i input polarization states with $i \in \{V, D, A, R, L\}$. (b) $\Delta F(\rho_{D,\text{out}}, \rho_{i,\text{out}})$ comparing the D and i input polarization states with $i \in \{H, V, A, R, L\}$. The uncertainty caused by imperfect polarization state preparation $\sigma = 0.057$ is indicated by the gray area.

of light is measured using a polarimeter (Thorlabs PAX1000IR1/M), which contains a rotating quarter-wave plate and a linear polarizer. The light is fiber coupled into the polarimeter using the appropriate fiber collimators.

First, we place the polarimeter before the light is coupled into the single-mode fiber (“input” box in Fig. 3.2) and calibrate the angles of the wave plates to obtain the six states of interest H, V, D, A, R, and L. We then send the light through the 200 m long fiber, and measure with the polarimeter the polarization after the fiber output ($\rho_{i,\text{out}}$) by averaging over 5 seconds with a sample frequency of 20 Hz. The input polarization states are permuted in the order H, V, D, A, R, L, and the process is repeated 10 times. We only want to test for unitarity of the fiber transformation, and we are not interested in the absolute output polarization state. Therefore, for every measurement, we calculate the fidelity $F(\rho_{j,\text{out}}, \rho_{i,\text{out}})$ of the output polarization states for different input polarizations, and compare to the expected fidelity from Eq. 3.9.

First, we discuss the measured fidelities for horizontal input $F(\rho_{H,\text{out}}, \rho_{i,\text{out}})$. The absolute fidelities are expected to be 0 for $i = V$ and $1/2$ for $i \in \{D, A, R, L\}$. The deviation from these expected fidelities, ΔF , is shown in Fig. 3.3(a) as a function of the duration of the experiment. We observe that most data points lie within the gray region, which

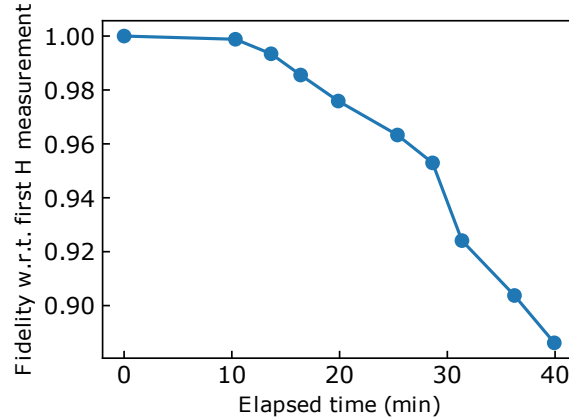


Figure 3.4: Fidelity $F(\rho_{\text{H,out}}(0), \rho_{\text{H,out}}(t))$ between polarization states exiting the fiber for an H-polarized input, shown as a function of elapsed time. The fidelity decreases by 11% over a span of 40 minutes.

represents the expected error arising from imperfect preparation of the input polarization states. Since the wave plates are adjusted manually, this error was quantified by repeatedly setting the same input polarization (H), measuring the outcome with the polarimeter, and then readjusting the wave plates. Repeating this process 10 times yielded an expected fidelity error of ± 0.057 . The errors of the polarimeter are below 0.25 degrees in both azimuth and ellipticity angles, which results in an inaccuracy of the fidelity of less than 0.0002. We can conclude that, within those errors, the 200 m fiber preserves the unitarity of the polarization states.

Fig. 3.3(b) shows the same analysis as Fig. 3.3(a), except that here the fidelity is calculated with respect to the incident D polarization: ΔF of $F(\rho_{\text{D,out}}, \rho_{i,\text{out}})$. We observe a similar result as in Fig. 3.3(a), demonstrating again preservation of unitarity. However, the deviations from the expected fidelity appear smaller than in Fig. 3.3(a), particularly when comparing HR and HL in Fig. 3.3(a) with DR and DL in Fig. 3.3(b). Since the measurements with incident D polarization are performed halfway through each measurement round, the temporal separation between the states used for fidelity calculations differs. The average time between the H and R measurements is 2.8 minutes, while it is only 1.3 minutes between the D and R measurements. These smaller deviations from the expected fidelity in Fig. 3.3(b) suggest a time-dependent change in the polarization transformation of the fibers, which we now proceed to investigate.

Figure 3.4 shows the time-dependent change in fidelity for horizontal input polarization $F(\rho_{\text{H,out}}(0), \rho_{\text{H,out}}(t))$, referenced to $t = 0$. We observe an 11% degradation in fidelity over a period of 40 minutes. This decline in fidelity confirms that the difference in spread of ΔF between the measurements in Fig. 3.3(a) and Fig. 3.3(b) can indeed be explained by time-dependent polarization changes.

In conclusion, a long single-mode fiber imposes a unitary transformation on the polarization states of light, as the fidelity between basis states remains unchanged. However, this unitary transformation changes in time, and re-calibration every couple of minutes might be required for experiments that rely on polarization stability.

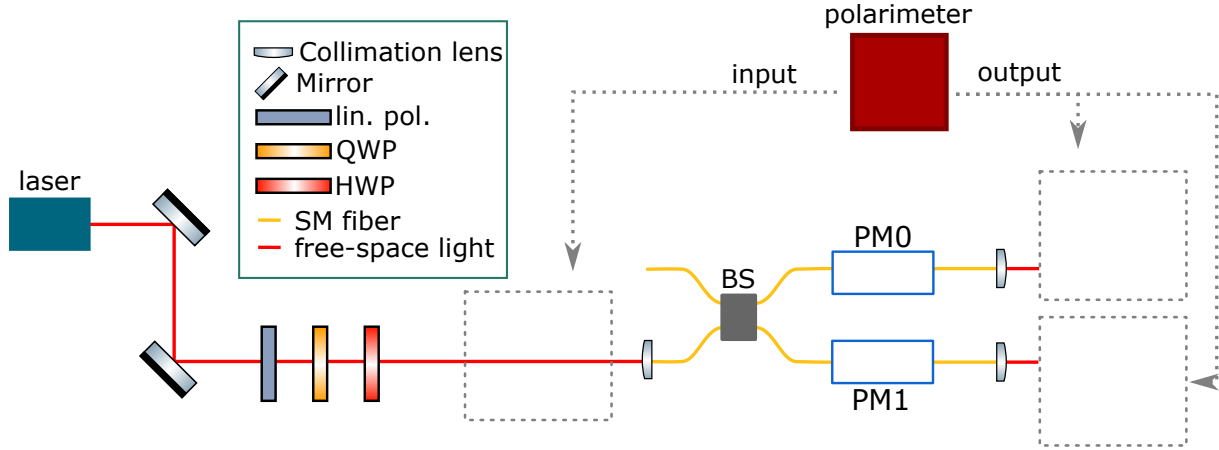


Figure 3.5: Schematic representation of the experimental setup, similar to the setup shown in Fig. 3.2, except that the long single-mode fiber is replaced with a fiber-based 50:50 beam splitter (BS) and two fiber-based polarization modulators (PM0 and PM1).

3.3 Unitary transformation of fiber-based polarization modulators

In a similar way, we investigate now the properties of fiber-based polarization modulators (PolaRITE III from General Photonics Corp.). These modulators are fully fiber-based (and therefore have low loss) and consist of four piezo-electric controlled squeezing actuators. Squeezing the optical fiber changes its birefringence and imposes a similar operation as a wave plate with tunable retardation. In the reference frame of the optical table, the first and third squeezers are oriented at 45° , while the second and fourth squeezers are aligned horizontally. Combined, the four squeezers enable full control of the output polarization state; any pure polarization state can be transformed into any other pure polarization state.

As with the long single-mode fiber discussed in Section 3.2, we first test whether the polarization modulators apply a unitary transformation to the polarization state of light. A similar experimental setup is used, shown in Fig. 3.5. The main difference is that the 200 m fiber is replaced with a non-polarizing 50:50 fiber-based beam splitter (Thorlabs TW850R5A2), with a polarization modulator (PM0 and PM1) positioned at each output to enable testing of the two modulators. The light exiting the polarization modulators is coupled into free space to allow the polarimeter to be inserted without disturbing the optical fibers in the setup. In addition, all fibers were secured to the optical table to prevent accidental movement, and a waiting period was introduced between setup and measurement to allow for relaxation. The measurement procedure is similar to the one discussed in Section 3.2. The input states (H,V,D,A,R,L) are adjusted in the same manner. We now change the voltage over the first squeezer from 0 to 5 V in steps of 0.05 V for each of the input states, and for each voltage step, the polarization state is averaged over 1 second at a frequency of 10 Hz with a total measurement time of around 2 minutes per polarization setting. We calculate the fidelities and average over the voltage. Fig. 3.6 shows for PM0 (a) and PM1 (b) the difference in measured fidelity $F(\rho_{i,\text{out}}(U), \rho_{j,\text{out}}(U))$ from the expected fidelity for input states i and j . Note that the case of $i = j$ is excluded

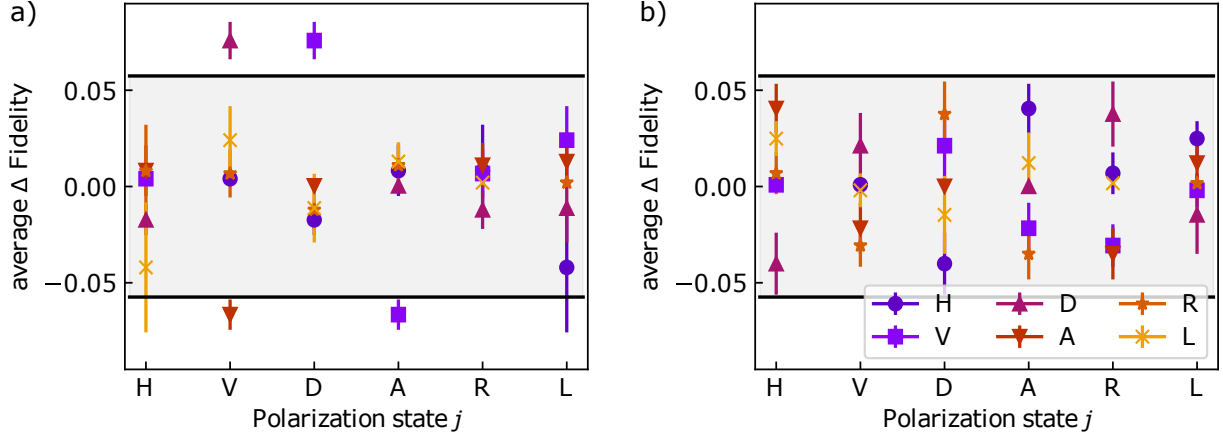


Figure 3.6: Deviation of the fidelity $F(\rho_{i,\text{out}}(U), \rho_{j,\text{out}}(U))$ between input state i and j from the expected fidelity, averaged over the squeezer voltage and for polarization modulator PM0 (a) and PM1 (b). The input polarization state j is indicated on the x-axis, and the markers indicate state i . The error bars show the statistical experimental errors from the polarization measurements, and the gray area indicates the expected error by the manual setting of the input polarization states.

as it results in $\Delta F = 0$. We see again that most measurements fall within the expected error range.

To conclude, by comparing the fidelity of the measured output states with the expected fidelities, we found that the squeezer-based polarization modulators induce unitary operations in polarization space, for any voltages applied to the squeezers.

3.4 Stability of fiber-based polarization modulators

To measure the temporal stability of our polarization modulators, we use the same setup as shown in Fig. 3.5. Instead of changing the voltage on a single squeezer, we now first apply a static voltage to two, three, or all four of the squeezers. After applying the voltage, the polarization state behind each polarization modulator is measured for a total time of 300 s in steps of 0.048 s. The squeezer voltages are set such that the polarimeter detects either horizontal (H) or vertical (V) polarized light. Although using all four squeezers allows full control of the output polarization state, H and V polarization can be reached with only two or three squeezers, if a suitable polarization state is chosen at the input of the modulator.

The results are presented in Fig. 3.7, which shows the change in measured fidelity ($F(\rho_i(0), \rho_i(t))$) relative to the first measurement point ($F = 1$) for both modulators. From these results, we observe an overall change in fidelity below a percent, 0.5% in the worst case, over a span of five minutes for PM0. For PM1, if 2 or 3 squeezers are used, the deviation in fidelity is similar to that of PM0, but when all four squeezers are in operation, the change in fidelity reaches a few percent.

Finally, we investigate the temporal evolution of polarization overlap between the two polarization modulators, a scenario directly relevant to the implementation of a two-photon QPV protocol. As before, we evaluate the fidelity of the measured polarization

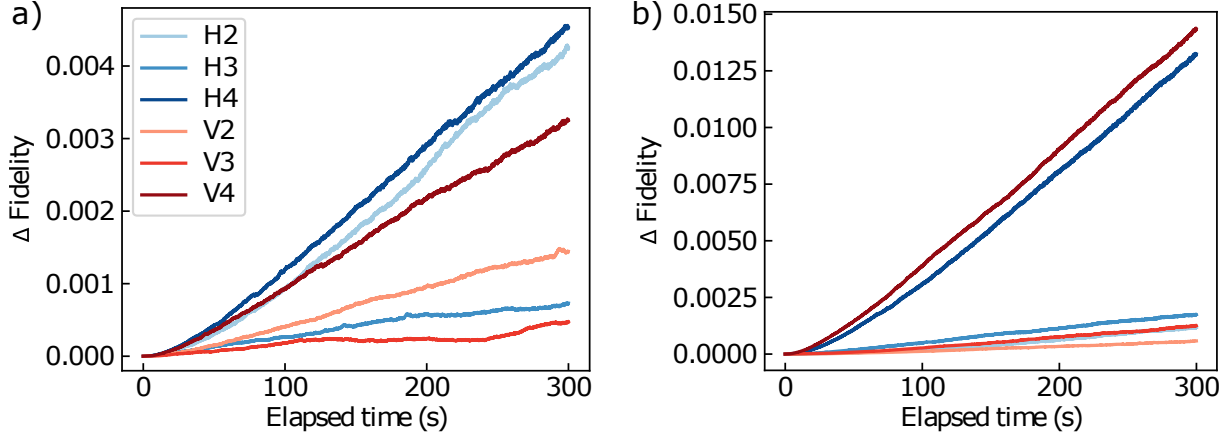


Figure 3.7: Deviation of the fidelity $F(\rho_i(0), \rho_i(t))$ from perfect polarization state overlap ($F = 1$) as a function of the elapsed time t for $i = \{H, V\}$ polarization, created with 2, 3, or 4 squeezers, for PM0 (a) and PM1 (b). The labels is indicate the polarization state i and the number of used squeezers s , for example, $i = H2$ means H-polarized light created using 2 squeezers.

states with respect to their expected values, but now for light exiting both PM0 and PM1 simultaneously. Fig. 3.8 shows the deviation of the fidelity $F(\rho_i(0), \rho_j(t))$ from the expected fidelity, where labels ijs indicate the combinations of input polarization states i, j , and the number of squeezers used s (which is the same for PM0 and PM1). Fig. 3.8(a) shows results for parallel polarization states with expected maximum overlap ($F = 1$), while Fig. 3.8(b) shows the results for orthogonal states (with expected overlap $F = 0$).

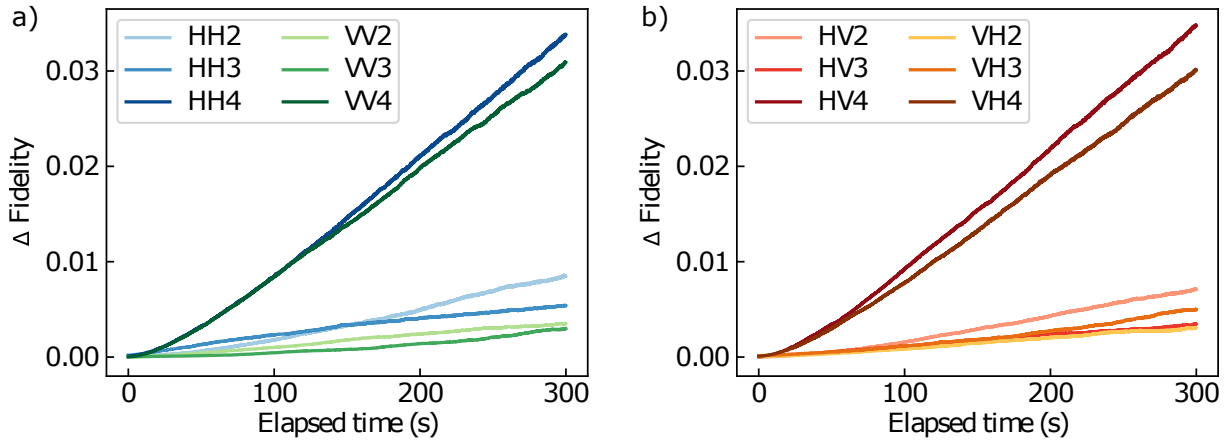


Figure 3.8: Deviation of the measured fidelity $F(\rho_i(t), \rho_j(t))$ from the expected fidelity as a function of time, for the case of equal polarization (a) where $F = 1$ is expected and orthogonal polarization (b) where $F = 0$ is expected.

We observe that the change in fidelity in Fig. 3.8 is larger than the shift in fidelity for each modulator individually in Fig. 3.7. This is expected, since the polarization changes of both modulators are independent, and this can lead to larger changes of fidelity. Fig. 3.8 shows that using all four squeezers generally results in the worst overlap between the states created by PM0 and PM1. This observation is corroborated by the fact that, particularly for PM1, this configuration exhibits the largest shift in fidelity over time, whereas using

three of the four squeezers produces a much smaller shift of approximately 1% over a 5-minute span. From these observations, we conclude that using three of the four squeezers generally provides the optimal static stability of the polarization states over prolonged periods, and using all four squeezers results in the poorest stability. However, it should be noted that the fourth squeezer may be necessary to prepare a desired polarization state.

3.5 Long term polarization fluctuations in a 200 m long single-mode fiber

Since a QPV demonstration experiment might run over several hours, we now investigate fiber-induced polarization changes over long periods of time, using the same experimental setup as shown in Fig. 3.2. Eight overnight measurements were taken over a span of 18 days, each having a duration of approximately 15 hours, and measurements were taken each 50 ms (day 1), 0.5 s (days 2, 3, and 9), and 1 minute. For the last five measurements, the lab temperature was recorded simultaneously using a Conrad TFD 128 temperature logger with an accuracy of 0.1 °C, positioned next to the optical fiber.

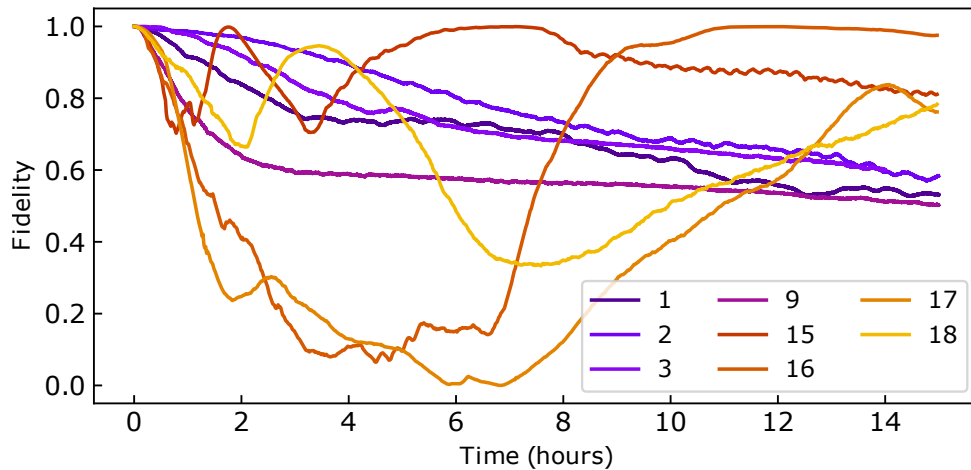


Figure 3.9: Polarization state fidelity $F(\rho_i(0), \rho_i(t))$ as a function of elapsed time t in hours measured over different nights in the span of 18 days (i).

Fig. 3.9 shows the evolution of the polarization state fidelity with respect to the polarization state at the start of the measurement. For the first four measurements (days 1-9), the fidelity decreases gradually towards approximately 0.5. In the final four measurements (days 15-18), the fidelity exhibits stronger fluctuations without a clear trend. This behavior cannot be attributed to fiber relaxation processes, since in that case the rate of change in fidelity would be expected to slow over time.

To investigate the unexpected fluctuations in fidelity in more detail, we focus on measurements taken on days 9 and 16. Fig. 3.10(a) and (b) show the evolution of the fidelity on these days, along with the corresponding state evolution on the Poincaré sphere. We observe that for day 9 the polarization state moves away from the initial point, first quickly and then more slowly, while for day 16 the polarization first moves away from the initial state but later returns to it. This becomes clearer in Fig. 3.10(c) and (d), where we show the velocity of the polarization state changes on the Poincaré sphere. We also show the measured lab temperature, and although the temperature changes are rather small in

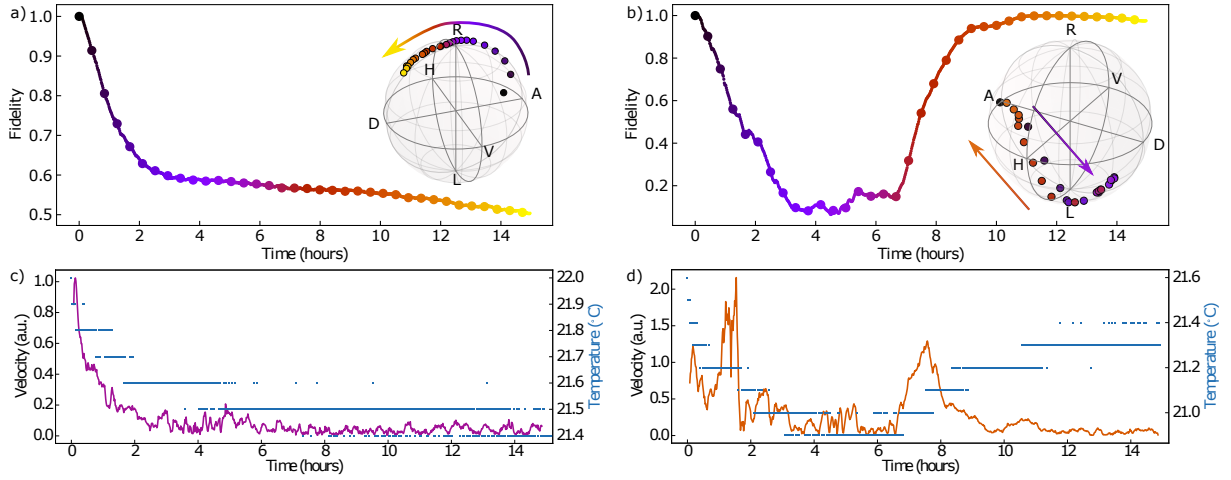


Figure 3.10: Fidelity $F(\rho_i(0), \rho_i(t))$ as a function of the elapsed time t for day $i = 9$ (a) and day $i = 16$ (b), the circular markers indicate points that are also shown on the Poincaré sphere in the inset, the arrow indicates the temporal evolution. Panels (c, day 9) and (d, day 16) show for the velocity of the polarization changes on the Poincaré sphere and the lab temperature measured simultaneously.

the order of $0.1\text{ }^\circ\text{C}$, we observe a clear correlation between temperature and polarization changes. We note that the initial relatively rapid changes in temperature and polarization are most likely caused by personnel leaving the laboratory.

Our results highlight the importance of temperature stabilization, but they also show that recalibrating the polarization, for example every 10 minutes, is sufficient to mitigate temperature-induced effects. The origin of these temperature-dependent polarization drifts has been investigated before and is most likely due to changes in strain in the optical fiber, which in turn modifies the strain-induced birefringence of said fiber [44].

3.6 Polarization mode dispersion in fibers

Polarization mode dispersion (PMD) describes a possible polarization-dependent group velocity of light during propagation in an optical fiber. If it is significant, it can pose serious limitations on using polarization qubits in quantum network protocols [45]. It is a frequency-dependent phenomenon that arises in fibers due to imperfections, stress, or geometrically induced birefringence such as a non-circularity of the fiber core, leading to distortion of propagating optical pulses [46].

To measure the PMD of our fiber, we use a so-called Müller matrix method (MMM) [47, 48] to determine the differential group delay (DGD) caused by PMD. In this method, two polarization input states are used to reconstruct the rotation matrix describing the polarization change by the optical fiber for two different optical frequencies ω_0 and $\omega_0 + \Delta\omega$. From this rotation matrix, the rotation angle is extracted, which in turn is used to calculate the DGD. We use vertical and anti-diagonal polarization as input states, which are described by the Stokes vectors \vec{t}_V and \vec{t}_A . In the experiment shown in Fig. 3.11, we prepare these states simply by using a linear polarizer in a computer-controlled rotation actuator. As the light source, we use a narrow-linewidth frequency-tunable continuous

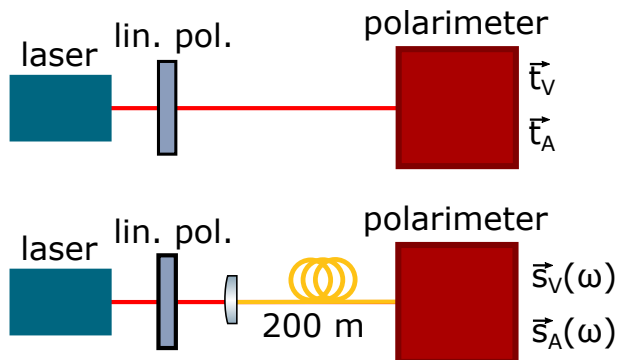


Figure 3.11: Schematic representation of measuring the input state \vec{t}_V, \vec{t}_A (top) and output states $\vec{s}_V(\omega), \vec{s}_A(\omega)$ (bottom) behind a 200m long 780HP optical fiber as a function of the wavelength of the frequency tunable continuous wave laser using a polarimeter.

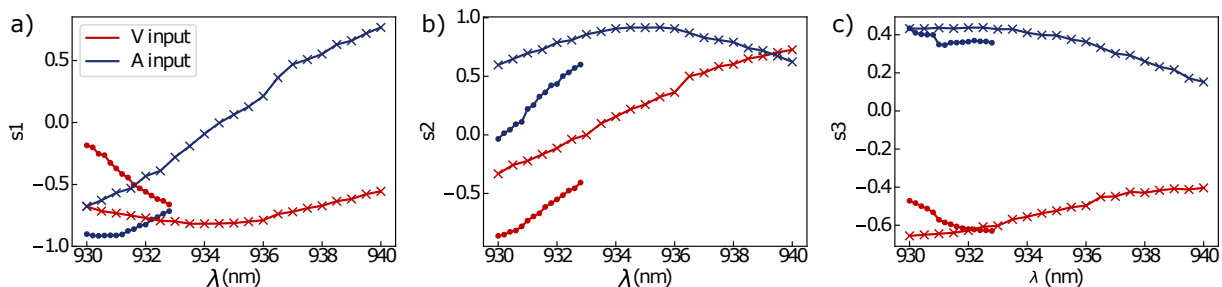


Figure 3.12: Normalized Stokes parameters s_1 (a), s_2 (b) and s_3 (c) as a function of the optical wavelength λ , for vertically (red) and anti-diagonally (blue) polarized input light for measurement 1 (\bullet) and measurement 2 (\times).

wave laser at around $\lambda = 930$ nm. We measure the polarization state at the output of the 200 m long 780 HP single-mode fiber using a polarimeter and obtain the Stokes vectors $\vec{s}_V(\omega)$ and $\vec{s}_A(\omega)$ for frequency ω . We discuss two measurements performed on consecutive days, where in measurement 1, the wavelength was tuned from 930.0 to 933.0 nm in steps of 0.2 nm, and in measurement 2, the wavelength was changed from 930.0 to 940.0 nm in steps of 0.5 nm. The optical wavelength was recorded using a spectrometer. For each wavelength and input polarization setting, the output polarization was averaged over approximately 5 seconds at a sampling frequency of 21 Hz. For each wavelength, the total measurement time, including changing of the laser frequency and polarizer adjustment, usually takes less than a minute, resulting in a total measurement time of 27 minutes for measurement 1 and 39 minutes for measurement 2.

Fig. 3.12 shows the wavelength-dependent normalized Stokes parameters calculated from the measured azimuth and ellipticity angles. We see that all three Stokes parameters experience a significant change over the measured wavelength range. We calculate the output Stokes vectors $\vec{s}_V(\omega)$ and $\vec{s}_A(\omega)$ from the Stokes parameters and use the Müller matrix method to calculate the differential group delay (DGD). First, for two laser frequencies ω and $\omega + \Delta\omega$, we calculate the polarization rotation matrices R that relate the output to the input polarization by $\vec{t} = R \cdot \vec{s}$ with a trick described by Jopson et al. [47], only requiring 2 input polarization states. Now we can calculate the difference rotation matrix that relates the output Stokes vectors at the two frequencies (the transpose of a

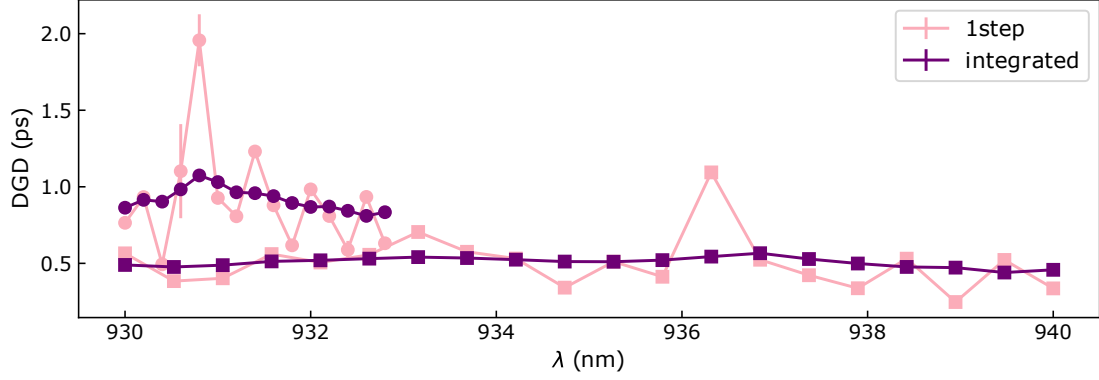


Figure 3.13: Differential group delay (DGD) as a function of the optical wavelength calculated using both the 1-step (pink) and integrated (purple) method. The DGD was calculated for both measurement 1 (●) and measurement 2 (■).

rotation matrix results in reversed rotation):

$$R_{\Delta} = R_{\omega+\Delta\omega}R_{\omega}^T \quad (3.10)$$

From R_{Δ} , we obtain the rotation angle ϕ from $\cos \phi = \frac{1}{2} (\text{Tr} R_{\Delta} - 1)$, and finally we obtain the DGD:

$$\Delta\tau = \frac{\phi}{\Delta\omega} \quad (3.11)$$

The experimentally obtained DGD is shown in Fig. 3.13 as a function of the optical wavelength λ , for both measurements. The DGD was calculated for neighboring measurements at ω and $\omega + \Delta\omega$ (“1 step”) or by calculating the DGD at ω with respect to every other frequency in the measurement and subsequent averaging over all values (“integrated”). The “integrated” method shows fewer variations due to the averaging.

The average DGD is 0.91 ± 0.05 ps (1-step method) and 0.92 ± 0.01 ps (integrated method) for measurement 1, and 0.503 ± 0.009 ps (1-step method) and 0.507 ± 0.002 ps (integrated method) for measurement 2. A possible explanation of this discrepancy is that the measurements were performed on two consecutive days, and it is known that environmental factors easily change the measured DGD [49, 50]. To compare to literature data, we determine the PMD coefficient in units of ps/ $\sqrt{\text{km}}$. This square-root length dependence originates in the fact that, in long fibers, different sections contribute in an uncorrelated way to the DGD. We obtain PMD coefficients of this fiber using the average DGD: 2.0 ± 0.1 ps/ $\sqrt{\text{km}}$ (1-step method) and 2.06 ± 0.02 ps/ $\sqrt{\text{km}}$ (integrated method) for measurement 1, and 1.12 ± 0.02 ps/ $\sqrt{\text{km}}$ (1-step method) and 1.134 ± 0.007 ps/ $\sqrt{\text{km}}$ (integrated method) for measurement 2. These PMD coefficients do fit within the broad range of values that can be found in literature [45, 47, 51–54].

Even if we consider the worst-case scenario for our 200 m fiber (DGD ≈ 2 ps), the broadening of the optical pulses is very small compared to the single-photon wavepacket lengths used in our experiments (around 50-100 ps). For longer fibers, however, PMD effects become relevant, for instance for a 10 km long fiber one can expect around 5 ps PMD, which would significantly decohere the polarization qubits and would require active stabilization [55, 56].